MicroRNA-155 Reduces Ventilator Induced Injury in Lung Epithelial Cells

Grant Chudik

Department of Biomedical Engineering

Spring 2019

Thesis Committee:

Dr. Samir Ghadiali, Advisor

Dr. Joshua Englert

Presented in Partial Fulfillment of the Requirements for Graduation with Honors Research Distinction in the Department of Biomedical Engineering at The Ohio State University

Abstract

Acute respiratory distress syndrome (ARDS) can be caused by a multitude of inciting events including trauma, sepsis, or pneumonia. During this condition, the bifurcating airways become occluded with fluid due to disruption of the alveolar-capillary barrier [1]. Mechanical ventilation is the necessary treatment for this condition, but the mechanical forces of ventilation have been shown to further exacerbate pre-existing lung injury, as well as activate pro-inflammatory signaling. Further injury due to ventilation is known as ventilator-induced lung injury (VILI) [2]. VILI consists of barotrauma, volutrauma, and atelectrauma. Specifically, atelectrauma is due to microbubble flow in the airway caused by the cyclic closure and reopening of the small airways. Microbubble flow can further disrupt the blood-oxygen barrier at the capillary walls due to shear forces. Recent clinical trials have focused on optimizing the ventilation forces to reduce injury. Although many therapies have been explored, the cell response to these forces has not been fully explored as a therapeutic target. When subject to mechanical forces, cells respond internally through the mechanotransduction pathway which can cause various downstream changes to the cell. The regulation of microRNA levels is one of the downstream changes that has been observed. MicroRNAs are small non-coding RNAs that regulate gene-expression, and several microRNAs have been shown to be associated with the lung epithelial cell response to injurious forces during mechanical ventilation including microRNA 155. To model VILI in-vitro, A549 lung epithelial cells were cultured in a flow chamber, which was used to subject the cells to micro-bubble flow. The main advantage of this in-vitro model is that it can replicate the complex mechanical forces exerted on lung epithelial cells during atelectrauma. To test the effect of microRNA expression on cell death, microRNA 155 was overexpressed in the A549 lung epithelial cells using transfection techniques. Pre-miR-155 transfected cells, as well as cells transfected with a scramble microRNA (negative control) and non-transfected A549s (control)

were cultured on separate 40mm slides until confluence was reached (>90%). Using these conditions, several experiments were carried out to test the effect of microRNA 155 overexpression on lung epithelial cells during ventilator conditions. Using a live-cell microscope, images of the cells were taken before and after to characterize detachment and cell death. The live/dead and detachment results from the control, scramble transfected, and 155 transfected cells were quantitatively compared. After exposure to five microbubbles the percent detachment did not differ significantly across the test conditions. The percent death did show a difference, with the microRNA 155 transfected samples showing significantly less death than the scramble and control samples. Based on the results of this experiment, microRNA 155 is shown to have a role in protecting A549 cells from bubble-induced stresses. These conditions have been shown to mimic the complex forces that have been observed in ventilator induced lung injury, meaning that microRNA-155 overexpression in lung cells may potentially have clinical significance. Future experiments will work to further characterize the role of miR-155 in lung epithelial cells using devices which more accurately model the in-vivo air-lung interface.

Acknowledgements

First and foremost, I would like to thank my research advisor Dr. Samir Ghadiali for giving me my first opportunity to become involved in scientific research. Without his guidance, none of the work that I've completed during my undergraduate years would have been possible. Through my experience working in his lab I have been able to develop so many valuable skills that I will be able to carry on with me into the future, and for that I will always be grateful.

I would also like to give thanks to my other mentors in the lab Chris Bobba, and Dr. Vasudha Shukla for teaching me everything I know in the lab and for being patient with me even when I was struggling. I'd also like to thank Dr. Englert for offering his opinions on my project in lab meetings and for advising me on my future endeavors. Furthermore, I'd like to thank the other students who I worked with in the lab including Youjin Cho, Tricia Oyster, Basia Gabela-Zuniga, Hyunwook Lee, and Yevgeniy Gladkiy for always supporting and helping me with whatever problems I was facing.

Additionally, I would like to thank my entire family, especially my Mom for supporting me throughout the years. Lastly, I would like to thank all of my friends who were always willing to listen to me complain about my school/lab work. Without the countless good times I've had with all of them, I would have never had the sanity to accomplish what I have been able to in my academic career.

Table of Contents

1. Background

1.1 Introduction

The lung is a highly complex organ consisting of a vast network of bifurcating airways which serve as the primary site of gas exchange in the body. The purpose of the intricate branching in the airways is to increase the surface area to volume ratio of the organ, making gas exchange efficient. In the less branched upper conducting regions of the lung, incoming air is warmed, and no gas exchange occurs. While in the lower, more branched respiratory regions, the lung tissue is much more compliant and stretches to allow the lungs to become filled with air. Gas exchange occurs at the end of the airways in what are known as the alveoli. The alveoli are small round structures which carry out gas exchange through their semi-permeable walls. The mechanism of breathing is carried out by the diaphragm muscle. Therefore, the tissues which make up the alveoli do not contain muscle cells and consist primarily of epithelial cells and connective tissues. Adjacent to the epithelial cells of the alveoli are the endothelial cells of the vasculature. Gas exchange occurs at this interface which is known as the alveolar-capillary barrier. The alveolar-capillary barrier consists of a basement membrane with epithelial cells of the alveoli on one side, and the endothelial cells of the capillaries on the other side. The semi-permeable nature of this barrier allows gas to flow from the lungs into the vasculature.

Although quite resilient and compliant, this barrier is susceptible to damage, which may lead to disruption of gas exchange in what is known as acute respiratory distress syndrome (ARDS). The primary risk factors for ARDS include, but are not limited to pneumonia, aspiration, and sepsis [1]. When the alveolar-capillary barrier becomes disrupted, gas exchange ceases due to the alveoli becoming filled with fluid from the extracellular space as shown in Figure 1-1 on the next page [1]. Recent studies have shown that up to 10% of all people admitted

into the ICU have ARDS [1]. The high incidence of ARDS shows the importance of developing treatment options for this condition. These patients suffer from hypoxia which leads to mechanical ventilation becoming the first line in treatment. Mechanical ventilation allows the respiratory muscles to relax while maintaining proper gas exchange.

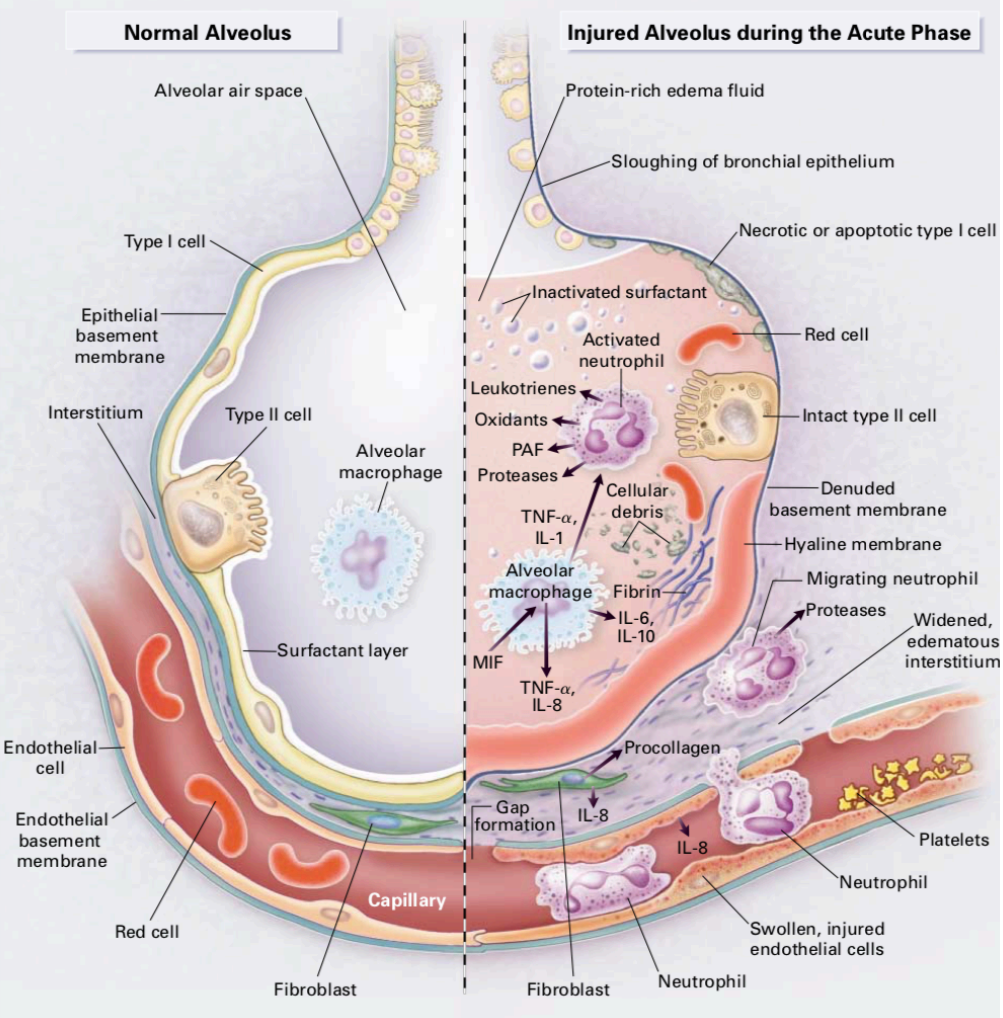

Figure 1-1 ARDS: The normal alveolar environment (left) compared to an injured alveolus during the acute phase of Acute Respiratory Distress Syndrome (right) [1].

Although there are clear benefits to using mechanical ventilation, the forces which it exerts on the lung can lead to further injury known as ventilator induced lung injury (VILI) [2]. Preventative measures for VILI have focused on optimizing the parameters of ventilation by altering the tidal volume and end-expiratory pressure. VILI is caused by several mechanisms including barotrauma, volutrauma, and atelectrauma. Barotrauma occurs due to the increased airway pressure which causes compressive forces on the lung epithelium. During high volume ventilation the lungs become overdistended causing further air leaks, known as volutrauma. Trials have shown that reducing the tidal volume results in a reduction of mortality by 22%, but lower tidal volumes have also been linked to injury caused by atelectrauma [3]. Atelectrauma occurs due to the repeated collapse and reopening of the alveoli causing shear forces which result in cell necrosis and detachment. Using positive-end-expiratory-pressure (PEEP), atelectrauma can be avoided, but this value varies on a patient-by-patient basis making proper treatment difficult [4]. The difficulty in developing proper ventilation techniques has led to further investigation of the mechanical forces which cause VILI, and how to mitigate these injurious effects through different means.

1.2 Mechanics and Morphology

When an ARDS patient is ventilated using low-volume ventilation techniques, the lung airways may close due to compliant collapse of small airways, or because of fluid occlusion in noncollapsed small airways [5]. During recruitment, air is pushed through the fluid occluded airways in order to reopen the lungs and provide oxygen to the circulation. As air is pushed through the fluid, the fluid-air interface of the propagating air bubble incurs normal pressure stresses, and tangential shear stresses on the airway walls. These forces are largely responsible for atelectrauma. As shown in Figure 1-2 on the next page, the propagating bubble results in a

hydrodynamic stress field applied to the lining of the lung epithelium [6]. The stress gradients induced cause epithelial cell necrosis and disruption of the alveolar-capillary barrier.

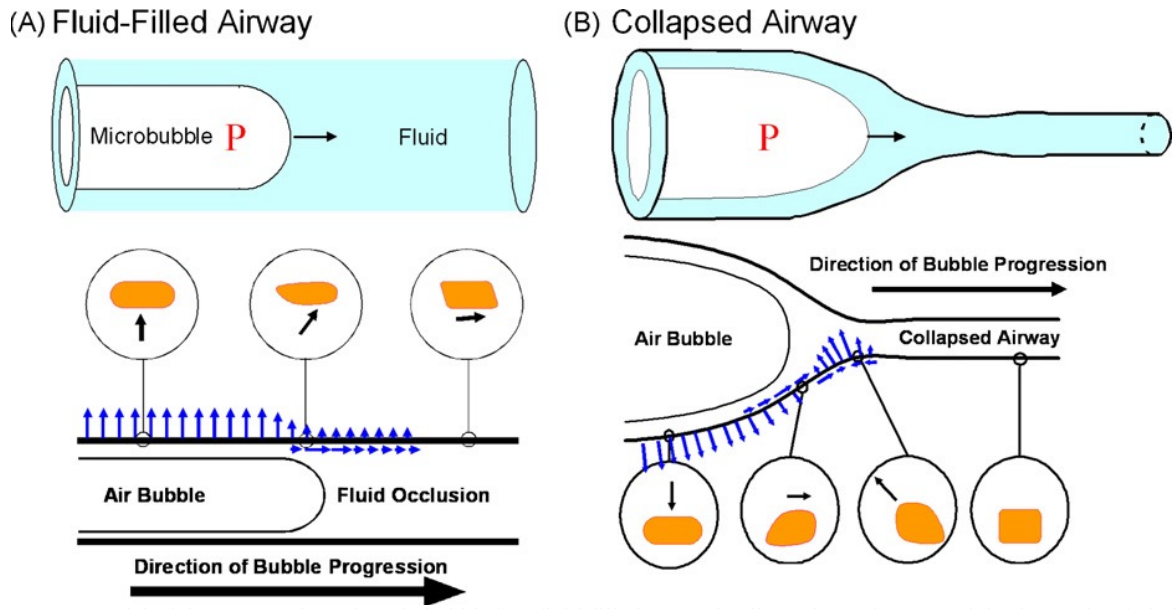

Figure 1-2: Model of the propagation of an air-bubble in a fluid-filled (A) and collapsed (B) airway, and the forces the air-bubble exerts on the lung epithelial cells [6].

Early in vivo models of rabbit ventilation demonstrated that both high and low inflation rates of lungs led to high inflammation rates and immune response [7]. Using the same model, these authors were also able to show that lower surface tension in the lungs led to less cell death, detachment and barrier disruption [8]. Whereas higher surface tension in the lungs demonstrated more cell death and pulmonary edema. Exogenous surfactant therapy can effectively reduce air-liquid surface tension but has had limited clinical success [9]. Alternatively, computational models have indicated that the epithelial cell morphology plays an important role in VILI. In a computational model of airway reopening, it was demonstrated that the hydrodynamic stresses on the epithelial cell may be a function of the cell's morphology [10]. Further computational models of the air-liquid interface interaction showed that a more compliant epithelial cell decreases the shear stress that causes cell injury [11]. Although membrane strain increased in

these models, the wall shear stresses were significantly lower, indicating that differences in cell softness may be able to decrease injury. Additionally, Maxwell and power-law rheology models of microbubble flow indicate that increased viscous damping results in less cellular injury [12]. In an in-vitro model using a parallel-plate flow chamber with a propagating air bubble to mimic airway reopening it was shown that decreased cell confluence resulted in more cell death [13]. The sub-confluent epithelial cells were longer and wider than the fully confluent cells, and their actin cytoskeleton was less fiber-like. Image-based computational models were used to investigate the mechanics of the sub-confluent cells compared to fully confluent cells under bubble flow conditions. These studies showed that the sub-confluent cells developed higher membrane strains, and that these strains decrease with increasing interior stiffness of the cell [14]. The primary way of altering the stiffness of the cell is by targeting the cytoskeleton. The cytoskeleton is what gives the cell is shape and rigidity, therefore depolymerizing it makes the cell much more compliant. Therefore, in-vitro experiments targeted the actin cytoskeleton to test whether its structural integrity (stiffness of the cell) had any effect on the epithelial cell death caused by bubble flow [15]. As seen in Figure 1-3 on the next page, actin stabilization had no effect on viability of the epithelial cells, but when depolymerized there was improved cell adhesion and viability. Overall, these experiments showed that cell stiffness is not a major determinant of injury, while changes in viscoelastic properties may play an important role in potentially mitigating the forces which cause VILI. By looking further into the way which the epithelial cells of the lung react to the forces of ventilation, and work to regulate their morphology, we may identify pathways that may be targeted to reduce injury.

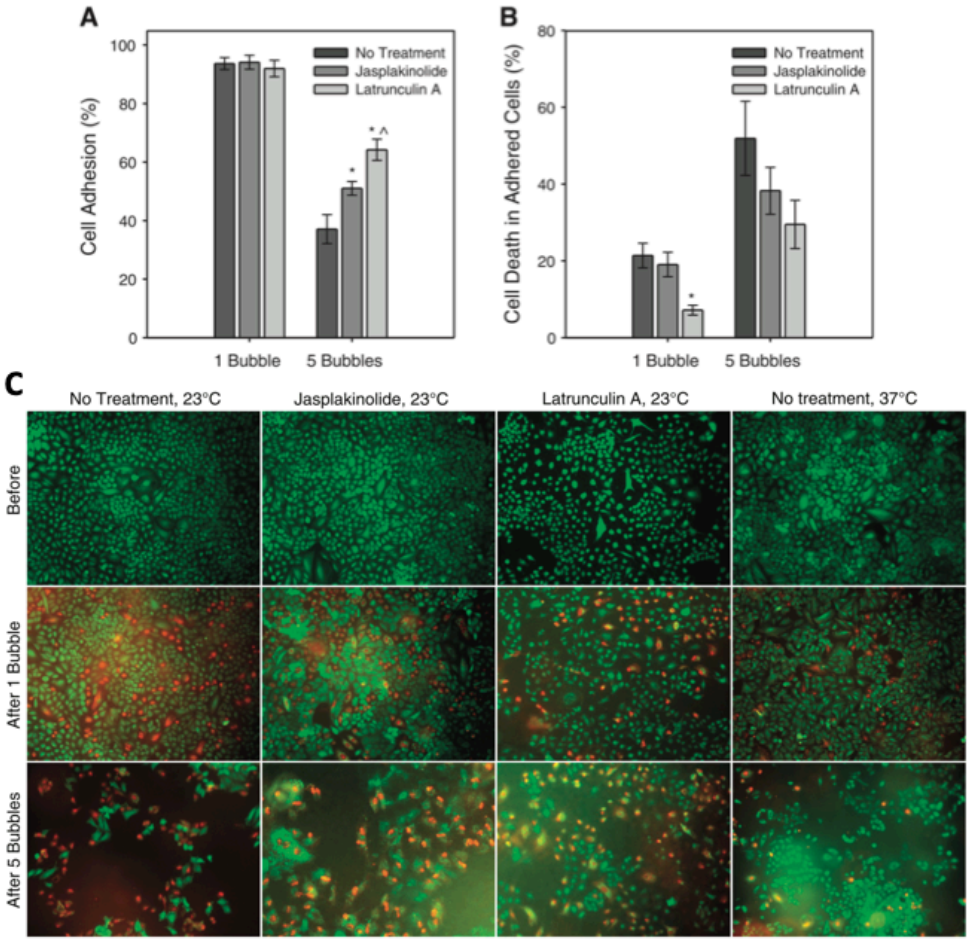

Figure 1-3 Actin Cytoskeleton Regulation: Actin cytoskeleton depolymerization (latrunculin treatment) significantly improves epithelial cell viability (A) and adhesion (B) when exposed to bubble flow. Representative live/dead fluorescent images of each test condition (C) [15].

1.3 Mechanotransduction

When cells are exposed to certain signals, a cascade of internal physiological events may occur, causing various downstream biochemical effects, many of which are unknown. Specifically, when this signal is mechanical in nature, the phenomenon is termed mechanotransduction. In epithelial cells, various mechanical forces have been identified as causing certain effects on the cell. When exposed to static transmembrane pressure, rat tracheal epithelial cells have been shown to increase expression for genes which regulate fibroblast growth [16]. Regulation of the cytoskeleton is one of the many responses that is also triggered by

external mechanical forces. Exposure of alveolar epithelial cells to shear stress has been shown to cause a time and stress dependent disassembly of the intermediate filaments [17]. Mechanical ventilation causes the cells to be exposed to complex hydrodynamic forces which in turn lead to a variety of mechanotransduced responses. One identified response of mechanical ventilation is the pro-inflammatory pathway, which was identified through cyclic closure and reopening ventilation in rats [18]. The epithelial cells response to ventilation forces was further identified using in-vitro models of oscillatory pressure which showed an increase in NF-κB activation [19]. NF-κB is a protein complex that regulates cytokine levels, DNA transcription, and cell survival. Depolymerization of the actin cytoskeleton in these experiments showed further activation of NF-κB. The inflammatory response to the forces of mechanical ventilation has been thoroughly investigated, however the role of microRNAs in the mechanotransduction response has recently become an area of interest.

MicroRNAs (miRNAs) are small (20-22 nucleotide) non-coding RNA molecules that function to negatively regulate post-transcriptional RNA. These regulatory molecules have been shown to play an important role in the pathogenesis of various diseases and have also shown promise to be used as a biomarker due to its disease specific regulatory nature [20]. Furthermore, microRNAs have been shown to involved in regulation of the inflammatory and apoptotic responses, which are common in VILI [21]. The changes in microRNA levels in response to mechanical ventilation was therefore investigated. Levels of miRNAs miR-155, miR-146a, and miR-21were all found to be significantly regulated as the result of mechanical ventilation [22]. These authors were also able to show that miR-21 is an important regulator of lung compliance in response to mechanical ventilation. Increased expression of miR-21 has also been shown to promote wound healing via inhibition of the PTEN pathway in rat skin cells [23]. In-vitro models which further explored the role of miR-146a during ventilator-like forces, showed that miR-146a

was up-regulated in human lung epithelial cells in response to oscillatory pressure [24]. Results of further experiments characterized the role of miR-146a in regulating the inflammatory response to mechanical ventilation. In endothelial cells, miR-155 has been shown to be upregulated in response to shear stress [25]. Additionally, it was concluded that miR-155 modulates the endothelial cell phenotype by downregulating RhoA, and MYLK expression, as well as actin cytoskeleton organization as seen in Figure 1-4. Yet the regulation of miR-155 has not been fully characterized in epithelial cell models.

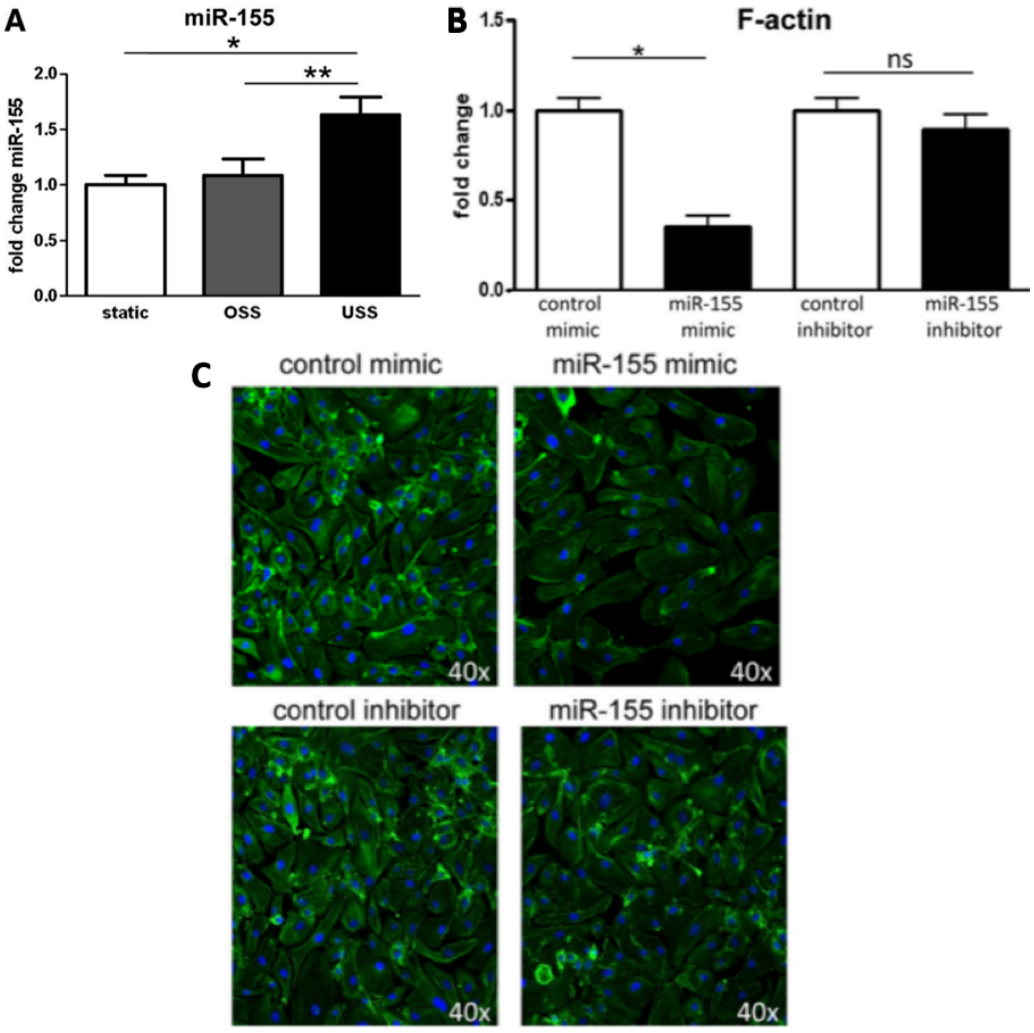

Figure 1-4 miR-155 Regulates Endothelial Cell Morphology: Increased miR-155 expression in endothelial cells exposed to shear stress (A). Decreased F-actin in endothelial cells transfected with miR-155 mimic (B) and representative fluorescent images of F-actin (C) [25].

1.4 Aims

The goal of this study is to identify the role of miR-155 in the lung alveolar epithelial cell's response to the forces of mechanical ventilation to see if it could be a potential therapeutic target for VILI. MiR-155 has been shown to be upregulated in lung epithelial cells when exposed to forces which mimic mechanical ventilation [22]. While in endothelial cells, upregulation of miR-155 in response to shear stress causes actin cytoskeleton depolymerization [25]. However, it is not known how altering the expression of miR-155 may change the epithelial cells response to the forces of ventilation. By further characterizing the role of miR-155 in the epithelial cell's response to ventilation we can gain a better understanding of how miRNAs regulate the epithelial cell, and if it's increased expression could be used for cytoprotective purposes. Keeping in mind that actin depolymerization in epithelial cells has been linked to decreased atelectrauma [15,26], we hypothesize that over-expressing miR-155 in lung epithelial cells will alter cell mechanics, decreasing atelectrauma. Through the use of in vitro modeling, we can attempt to replicate the forces of ventilation on a smaller scale to study atelectrauma on cultured epithelial cells. Transfection delivery methods can be used to alter the intracellular concentration of miRNA in order to study the effects of increased and decreased concentration. Through determining the role of miR-155 we can gain a better understanding of VILI and can identify a therapy which may show cytoprotective abilities, mitigating the injury associated with ventilation.

2. Materials and Methods

2.1 Cell Culture

The adenocarcinomic human alveolar basal epithelial cell line (A549) was used throughout this study to model lung alveolar epithelial cells. A549 cells were kept in cell culture flasks at incubation conditions (37^{o} C, 5% CO_2, 95% humidity) with high-glucose (4.5 g/l) Dulbecco's Modified Eagle Medium (DMEM) supplemented with 10% fetal bovine serum (FBS) and 5% Antibiotic/Antimycotic (Anti/Anti). Once A549 cells reached full confluence in their respective culture flasks, they were detached using TrypLE express enzyme 1X (trypsin) by removing the DMEM and replacing it with trypsin. After incubating the trypsin for 7-10 minutes, an equal amount of DMEM was added to the flask to deactivate the trypsin. The cell solution was then removed from the culture flask and centrifuged in 15 mL tubes at 1100 RPM. The supernatant was then removed, and the pellet was resuspended in supplemented DMEM. The cell suspension could then be used to seed the A549 cells in new tissue culture flasks and dishes.

2.2 Bubble Flow Apparatus

Atelectrauma is caused by repetitive closure and re-opening of alveoli causing the occurrence of micro-bubbles which exert shear forces on the epithelial cells. To replicate the atelectrauma that mechanical ventilation causes, a bubble flow apparatus was used to subject the A549 epithelial cells to repeated microbubble flow. The flow apparatus used was the FCS2 System provided by Bioptechs shown in Figure 2-1 on the next page. The channel has a length of 20 mm, width of 10mm and height of 500 μm. To prepare the apparatus, 40mm coverslips were placed in 60mm culture dishes and submerged in 70% ethanol for 20 minutes. The ethanol was then aspirated, and the 40mm coverslips were transferred to new sterile 60mm culture dishes. A549 cell suspension was then added to the 60mm culture dish on top of the 40mm coverslip, along with additional supplemented DMEM to reach a final volume of 4 mL. Once cells had

grown to ≥ 90% confluence on the 40mm coverslip, the chamber assembly components were submerged in 70% ethanol for 20 minutes, and then were removed and allowed to dry. The 40mm coverslip cultured with A549s was then removed from the 60mm dish and assembled into the apparatus as shown below (with cell side facing up). Two tubes were then attached to either side of the assembly. One of the tubes was attached to a 0.2 um filter, while the other was attached to a 5 mL Hamilton gastight syringe filled with Phosphate Buffered Saline (PBS). PBS was used instead of cell media because of its higher surface tension properties. These properties allowed for smoother propagation of the microbubble.The syringe was then assembled into a syringe pump set for the specifications of the syringe. With a refill/infuse speed of 1 mL/min and air bubble could then be propagated and retracted over the A549 cell monolayer. Images of the cells were taken by mounting the apparatus on an inverted fluorescent microscope. Differential interference contrast (DIC) channels were used to obtain high contrast images of the cells. To image live/dead cells, samples were stained with calcein (live) and ethidium (dead). The stains were diluted using PBS (calcein- 1000X, ethidium-500X). Fluorescein (FITC) and cyanine 3 (CY3) microscopy channels were used to obtain live/dead images. Image analysis was carried out using ImageJ software.

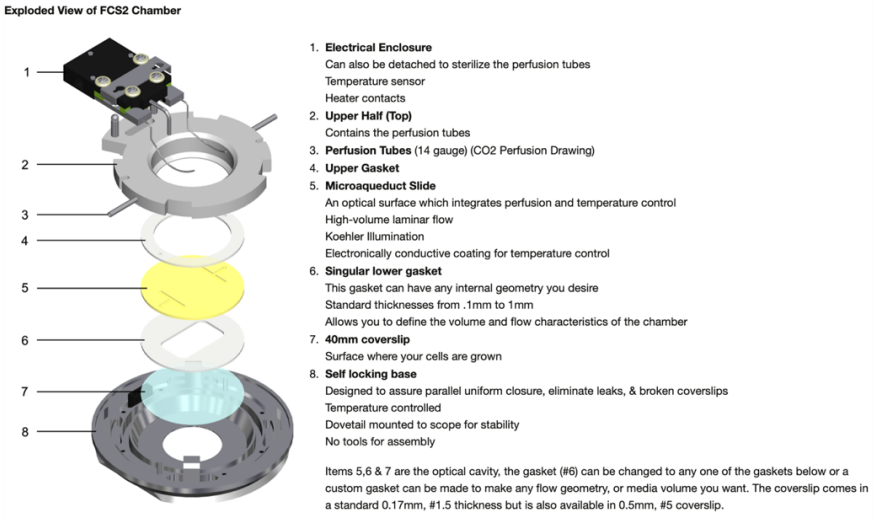

Figure 2-1: Bubble flow apparatus components and assembly.

2.3 MiRNA Transfection

In order to alter miR-155 concentration, A549 cells were forward transfected with either pre-miR-155 vector or pre-scramble vector (negative control). A549 cells were first allowed to grow to ~50% confluence in their respective culture dish. Stock vector solution (1μM) was diluted using reduced serum medium (optimem) to 0.5 nM while lipofectamine was diluted with optimem using a 1:50 ratio (lipofectamine:optimem). The dilute lipofectamine solution was then incubated for 5 minutes, mixed in equal parts with the vector solution, and then incubated an additional 15 minutes. DMEM was then removed from the ~50% confluent sample, and the vector/lipofectamine solution was added along with optimem to dilute using a 1:6 ratio. For 40mm coverslips, a final volume of 2.4 mL was used while for 6-well plates a 1.2 mL final volume was used. Six hours later the transfection solution was removed and replaced with supplemented DMEM. 24 to 48 hours later the sample could then be used for experiments.

2.4 Polymerase Chain Reaction

To measure miRNA levels in the A549 epithelial cells polymerase chain reactions were used to amplify RNA content and analyze levels. Using a standard trizol RNA isolation protocol, RNA was extracted from A549 triplicate samples of each of the following conditions: control, scramble transfected, and miR-155 transfected. The RNA concentration of these samples was then determined using nucleic acid quantification nanodrop technology. Once concentration was determined, each sample was diluted to 25 ng/mL using RNAse free water. Complementary DNA was then generated from the samples by combining the samples (nucleic acid) with a cocktail of solutions specified in Table 2-1 on the next page.

	per sample (µL)	
	miRNA→cDNA	mRNA→cDNA
dntp (blue)	0.075	0.8
inhibitor (white)*	0.095	1
RT enzyme (purple)	0.5	2
buffer (yellow)	1	1
primer	1.5 (specific primer 5X)	1.5 (random primers)
RNAse free H2O	5.925	9.7
total before nucleic acid	9.095	16
extracted RNA	~1 (25ng)	~4 (100ng)
total	10.095	20

Table 2-1: Solution mix for complementary DNA protocol.

Once samples were prepared, they were loaded into the thermocycler, and ran on a heating program based on the RNA molecule being amplified. For miRNA: 16°C , 30m → 42°C, 30m → 85°C, 5m → 4°C, ∞. For mRNA: 25°C , 10m → 37°C, 120m (do 2 sets of 60m when entering program) → 85°C, 5m → 4°C, ∞. Finally, a standard quantitative PCR protocol was used with a Roche Light Cycler 480 to determine levels of miRNA or mRNA. Samples with miR-155 probe were normalized against samples with U18 control probe. MiR-155 transfected samples as well as scramble transfected miR-155 levels were then normalized against the control samples to obtain a fold difference.

2.5 Western Blotting

Western blotting experiments were used to examine whether miR-155 transfection caused a decrease in specified protein content. Triplicate A549 samples of each of the following condition were used for the blot: control, scramble transfected, and miR-155 transfected. Cell samples were first cultured and transfected in 6-well plates. After the transfection procedure was complete, each of the samples were washed with PBS, then lysed using

radioimmunoprecipitation assay (RIPA) buffer cocktail. The recipe for the RIPA buffer cocktail consisted of 500 μL RIPA buffer, 75 μL mini protease inhibitor cocktail, 5 μL PMSF protease inhibitor, and 5 μL of phosphatase inhibitor. Cells were scraped, collected and centrifuged at 13,000 g for 10 min at 4° C. The supernatant for each sample was collected. Using a Pierce BCA Protein Assay Kit and standard plate reader, the protein content of each sample was quantified. The protein was then diluted using the RIPA buffer cocktail, so each sample contained 25 μg of protein. Samples were then prepared by diluting 4X with LDS buffer, and heating at 70° C. Samples were ran on a 4-12% Bis-Tris Protein gel at 150V for 40 minutes. The gel was then assembled into a transfer cassette along with nitrocellulose membrane, and was run at 20V for 1 hour. The nitrocellulose membrane was then stained with ponceau to confirm the transfer had occurred. After repeated rinsing of the membrane with a mixture of tris-buffered saline and polysorbate 20 (TTBS), the membrane was submerged in 5% milk for 1 hour for blocking purposes. The primary antibody of the desired protein was then mixed with 5% milk (RhoA 1:1000, MYLK 1:1000, B-actin 1:5000, GAPDH 1:2000) for a final volume of 3 mL, and was placed in a 50 mL tube with the membrane. The tube containing the membrane and primary antibody was then placed in a rotator overnight. The next day, the membrane was removed from the tube and rinsed several times with TTBS. A 5 mL mixture of 5% milk and corresponding secondary antibody (Rabbit 1:3000, Mouse 1:5000) were added to the membrane. After 1 hour, the membrane was rinsed with TTBS and imaged using Supersignal West Pico Plus Chemiluminescent Substrate.

2.6 Traction Force Microscopy

Traction force microscopy (TFM) was used to measure the contractile forces generated by A549 cells. MiR-155 transfected A549 cells were compared against untreated control A549 cells. To run TFM, polyacrylamide gels with embedded red fluorescent carboxylate-modified beads with diameter of 0.5 μm were prepared on 25mm glass cover slips. These gels were then coated with bovine collagen type I using UV light and crosslinker sulfo-SANPAH. A549 cells were then seeded at low density on the collagen coated polyacrylamide gels. An inverted fluorescent microscope was used for imaging. Phase contrast images of single cell boundaries and fluorescent images of the underlying beads were captured before and after the cells were treated with cellular dissociation solution, trypsin. Bead displacement was calculated using correlation-based particle image velocimetry (MATLAB) which uses bead location data before and after trypsin exposure. Individual cell tractions were then calculated from the displacement and cell boundary data using finite element modeling (COMSOL).

2.7 Atomic Force Microscopy

A549 cells were cultured on 40 mm glass coverslips. Samples were either control or were transfected with miR-155. Once confluent, glass coverslips were mounted in 60 mm culture dishes with immune-mount (incubate at 37^{o} C for 1 hour, no light). Samples were then immersed in sterile saline and atomic force microscopy performed. Stiffness measurements were performed using Asylum MFP-3D Bio AFM mounted on an inverted fluorescent microscope. Cell samples were indented using silicon nitride cantilevers with a 10 μm polystyrene spherical tip and nominal spring constant of 0.01 N/m. Force maps at 5–10 regions of 20μmx20μm were collected and approximately 250–300 force-displacement curves were analyzed per sample for each matched pair (control and miR-155 transfected) experiment. Force curves were analyzed using the Oliver-Pharr model to compute the tissue Young's modulus [27].

2.8 Cytoskeletal Imaging

To investigate potential differences in the actin cytoskeleton, untreated and miR-155 transfected A549 cells were seeded onto 25 mm glass coverslips at low density. To prepare for imaging, the glass coverslips were submerged in 10% formalin (3.7% formaldehyde) for 10 minutes. Samples were then washed multiple times with PBS (0.1% triton) for 10 minute each. Phalloidin (1:40 dilution from methanolic stock) was then placed on the samples for 45 minutes (protected from light). After an additional three washes with PBS, samples were treated with the blue fluorescent DNA stain DAPI (1:10,000 dilution from stock) for 5 minutes. Additional washes with PBS were then carried out and the coverslips were mounted in 60 mm culture dishes with immuno-mount (incubate at 37^{o} C for 1 hour, no light). Fluorescent imaging was then carried out on an inverted fluorescent microscope.

2.9 MTT Cell Proliferation Assay

The effect of miR-155 overexpression on A549 cell proliferative ability was tested using an MTT proliferative assay. 12 mM MTT stock solution was prepared by adding 1 mL of sterile PBS to one 5 mg vial of MTT (Vybrant MTT Cell Viability Assay), and vortexing until dissolved. SDS solution was then prepared by adding 10 mL of 0.01 HCl to a tube of 1 gm of SDS. Pre-miR-155 transfected, pre-scramble transfected, and non-transfected A549 cells were seeded in a 96 well plate at 7,500 cells per well. Next, 10 µL of 12 mM MTT stock solution was added to each well. Cells were then incubated at 37^{o} C for 4 hours, and then 100 µL of SDS-HCl solution was added to each well. After an additional 4 hours of incubation, the solutions were mixed and the absorbance at 570 nm was read on the plate reader. Absorbance values were then used to quantify the cell proliferation rate. Samples were normalized to a control absorbance (no cells), and then transfected samples were normalized to the untreated samples.

2.10 Statistical Analysis

Data from the resulting experiments was analyzed statistically to determine the significance of the results. First, the distribution of the data was analyzed for normality. If the data passed the test for normality (Shapiro-Wilk), the distribution was not altered. If it did not pass a normality test, then the data was log-transformed and analyzed again for normality. For data sets which contained two test conditions, a two-sample t-test was conducted. While for the experiments which included more than two test conditions, a one-way ANOVA with a post-hoc Tukey test was conducted for group comparison. Any experiment which was done over time was statistically analyzed using an ANOVA with repeated measures. P-values were obtained and were concluded to be significantly different if the P-value was less than 0.05.

3. Results

3.1 MiR-155 Expression Post Transfection

To test the ability of the miRNA transfection to effectively increase the expression of miR-155 in A549 lung epithelial cells, quantification was carried out using PCR techniques previously described. Triplicate samples of A549 cells in each of the following conditions were tested: control, pre-scramble transfected, and pre-miR-155 transfected. Gene fold levels of miR-155 in the samples were normalized against U18 control levels. Samples were then normalized to the control conditions to obtain the values shown in Figure 3-1 below. Levels of miR-155 were slightly decreased in pre-scramble transfected conditions compared to control conditions. While miR-155 transfected cells showed a 200-fold increase in miR-155 levels compared to control conditions.

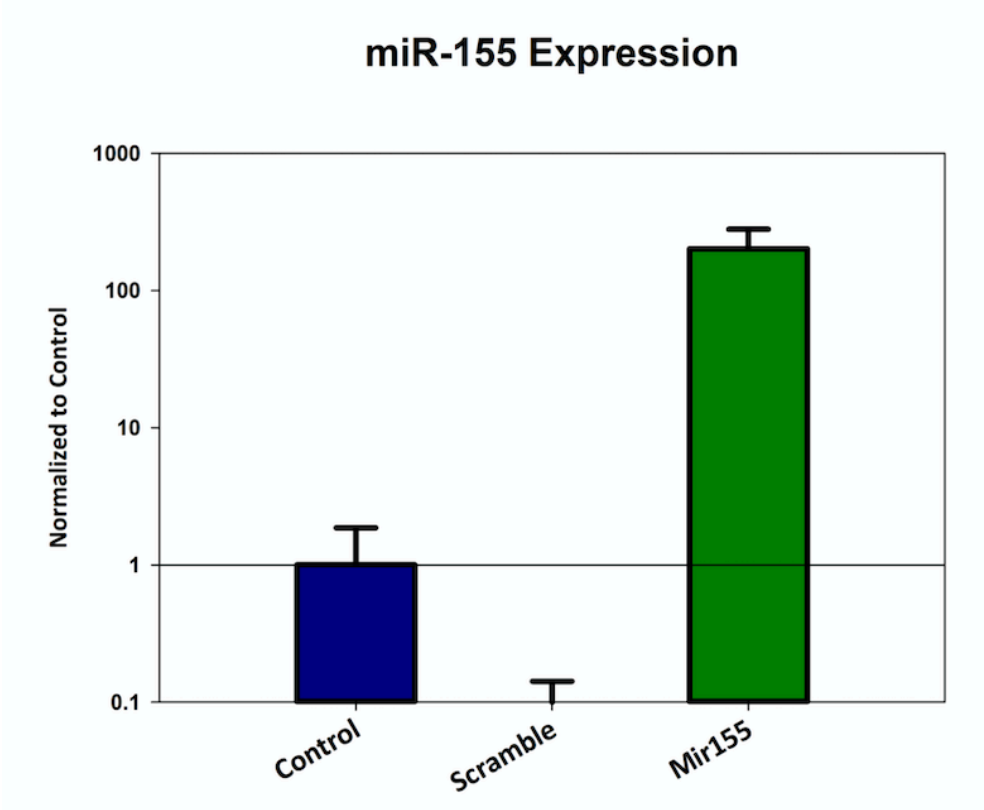

Figure 3-1: PCR Analysis of miR-155 Expression for control conditions (blue), pre-scramble transfected (red), and pre-miR-155 transfected A549 cells.

3.2 Bubble Flow Induced Injury to A549 Cells

To see if miR-155 expression has a protective role in lung epithelial cells exposed to ventilator-like forces, A549 cells with varying miR-155 expression levels were exposed to repeated bubble flow. Triplicate samples of pre-miR-155 transfected, pre-scramble transfected (negative control), and untreated A549 cells (control) were used. Samples were exposed to 5 bubble flows at a flow rate of 1 mL/min. Live and dead cells from each sample were then quantified. Average percent death across samples was determined and the average ± standard deviation for each condition is shown in Figure 3-2 along with representative fluorescent live/dead images of pre miR-155 transfected and control conditions. Pre miR-155 transfected samples showed significantly less cell death than both control (P = 0.01) and pre-scramble transfected (P = 0.005) samples. There was no statistically significant difference between control and pre-scramble transfected samples.

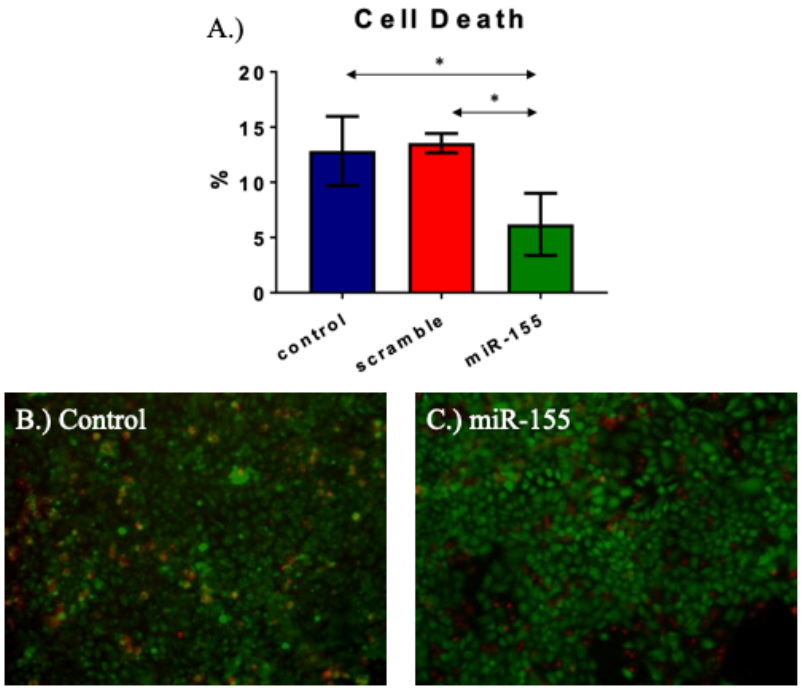

Figure 3-2 Bubble Flow Induced Cell Death: A.) Quantification of percent cell death after exposure to bubble flow. B.) Fluorescent Live/Dead Image of a control sample. C.) Fluorescent Live/Dead Image of a pre-miR-155 transected sample. * Indicates statistically significant difference.

Epithelial cell detachment (component of VILI regularly seen in conjunction with cell necrosis) was quantified in a similarly set up, but separate experiment. Triplicate samples of the three previously described test conditions were subject to 20 bubble flows at a flow rate of 1 mL/min. Samples were imaged before and after exposure to bubble flows. Average cell detachment across sample conditions was determined and the average ± standard deviation for each condition is shown in Figure 3-3 along with representative high contrast images of each test condition. There was no statistically significant difference between the different treatment conditions (P = 0.254).

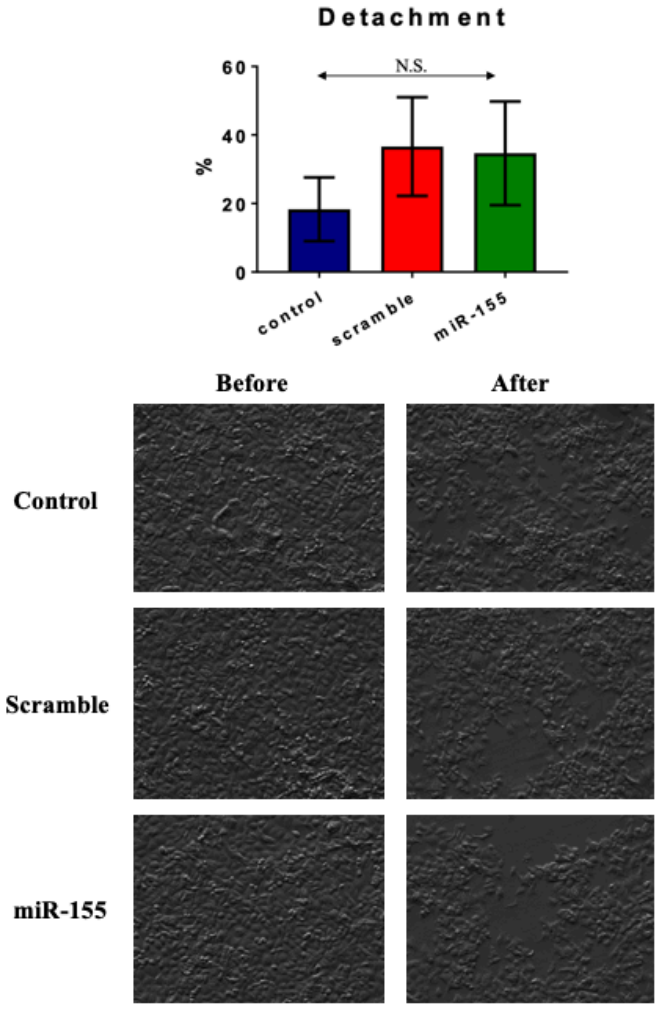

Figure 3-3 Bubble Flow Induced Cell Detachment: Quantification of cell detachment after exposure to bubble flow (top). Representative images of cell monolayer for each condition before and after exposure to bubble flow (bottom). N.S. indicates no statistical significance.

3.3 Wound Repair Following Injury

In order to see if miR-155 expression has an effect on VILI wound repair, tests on re-growth (migration) of an epithelial cell monolayer after bubble flow injury were carried out. Samples for this experiment consisted of triplicates of untreated, latrunculin treated, and pre-miR-155 transfected A549 cells. Bubble flow and microscopy were used to expose samples to bubble flow until ~50% confluence of the monolayer was reached. Images were then taken over the span of 48 hours as the monolayer regrew. Confluences for each condition at each time point were averaged and the average ± standard deviation values were used to make the line graph seen in Figure 3-4 below. Differences between regrowth were not seen to be statistically significant based on results from the repeated measures ANOVA ($P > 0.05$).

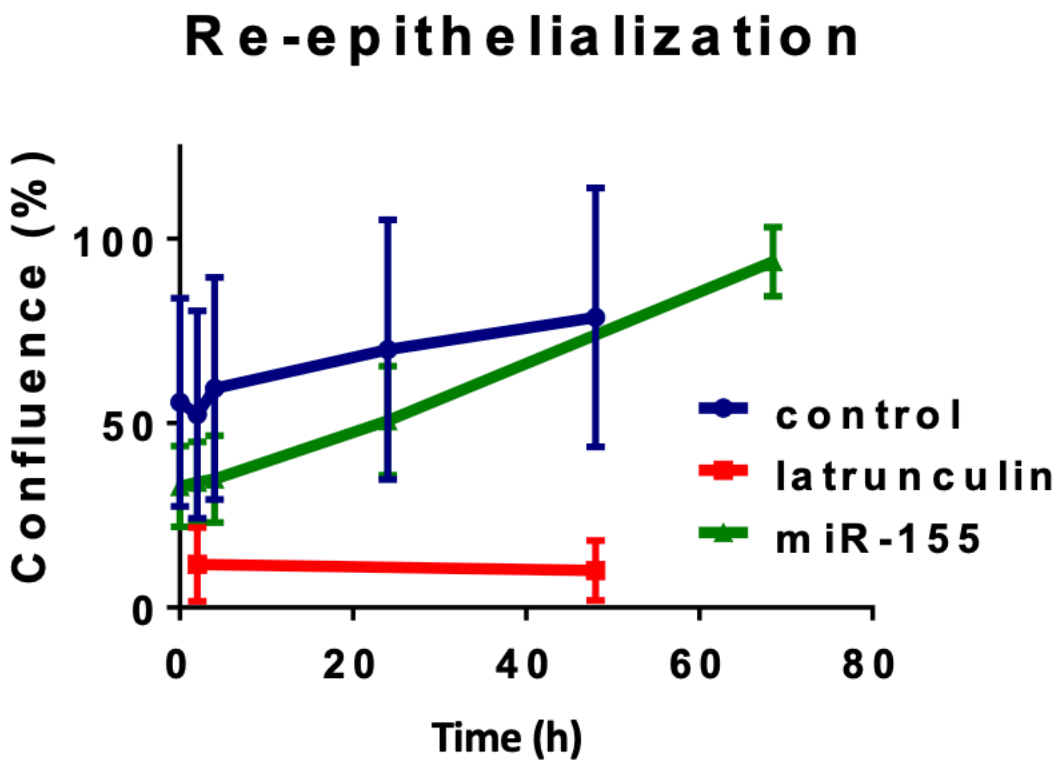

Figure 3-4 Re-Epithelialization After Bubble Flow Induced Injury: Confluence measurements as a function of time for untreated A549s (blue), latrunculin treated A549s (red), and pre-miR-155 transfected A549s.

The effect of miR-155 overexpression on wound repair was further characterized through analysis of the A549 proliferative ability. Using an MTT Cell Proliferation assay, absorbance values were collected for samples of pre-miR-155 transfected, pre-scramble transfected, and untreated A549 samples. Absorbance values correlated with cell proliferative activity. The absorbance for treated samples was normalized against the control to obtain relative proliferative ability. The P-value was greater than 0.05, therefore no statistical significance in levels was seen. The relative levels of proliferative ability normalized to control are seen in Figure 3-5.

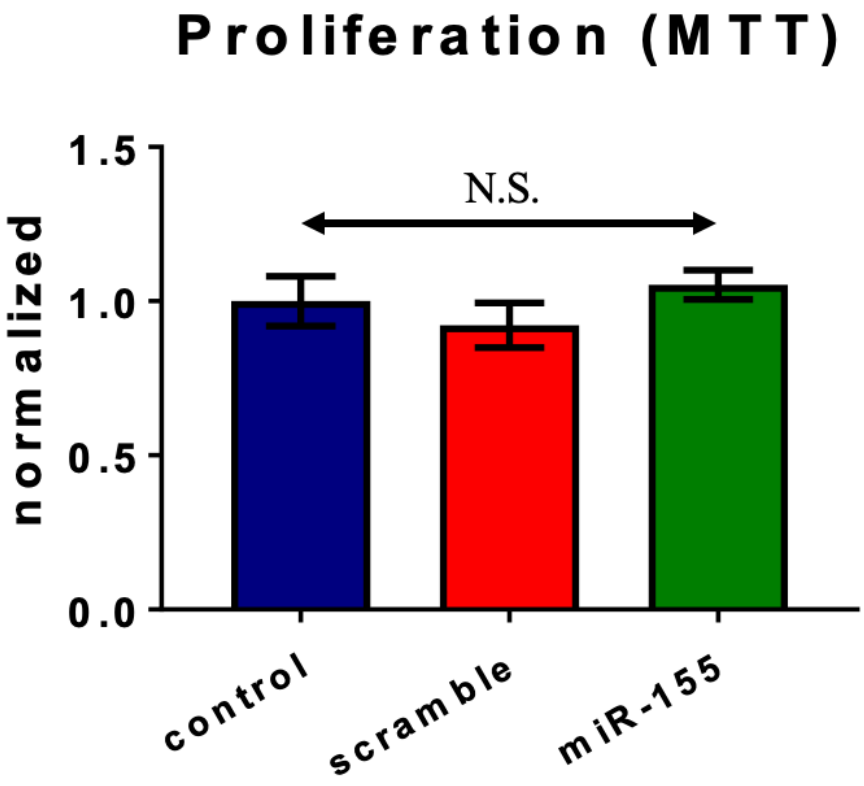

Figure 3-5 MTT Proliferation Assay: Proliferative ability of pre-miR-155 transfected (green), and pre-scramble transfected (red), normalized to the control (blue).

3.4 Cell Morphology

MicroRNAs are capable of regulating various aspects of the cell including morphological properties. Changes in morphological properties have been shown to alter epithelial cell susceptibility to VILI. Atomic force microscopy (AFM) was conducted to determine if miR-155 overexpression affects a change in the morphology that may be responsible for the decreased susceptibility to injury from ventilator-like forces previously seen (Figure 3-1). Multiple samples of untreated, and pre-miR-155 transfected A549 cells were tested. Average young's modulus and cell height across sample conditions were determined and the average ± standard deviation for each condition is shown in Figure 3-5 along with representative deflection tracings of each test condition. A statistically significant decrease in young's modulus and increase in cell height was observed for pre-miR-155 transfected samples ($P<0.001$).

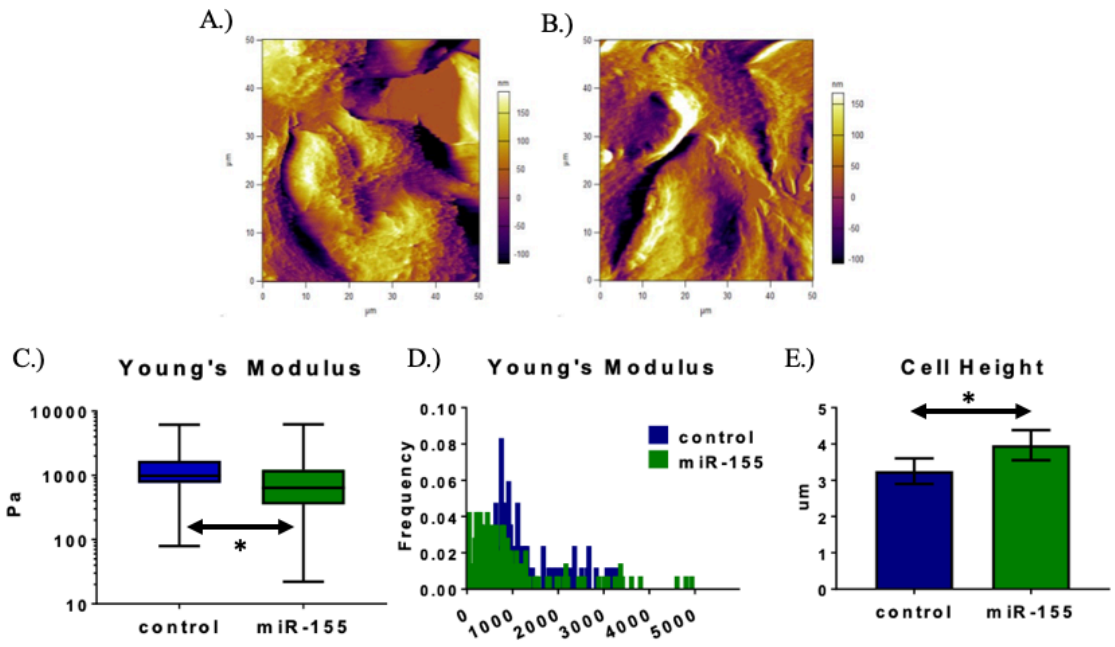

Figure 3-5 AFM Analysis: Representative deflection tracings of pre-miR-155 transfected (A) and untreated (B) A549 cells. Plots of young's modulus values (C, D) and cell height (E) for pre-miR-155 transfected (green) and untreated (blue) A549 cells. * Indicates statistically significant difference.

To further characterize any potential morphological changes in the pre-miR-155 transfected cells traction force microscopy was done to quantify the contractile forces which the cell exerts. Samples of untreated, pre-scramble transfected, and pre-miR-155 transfected A549 were used. For each sample, the contractile forces of ~20 cells were measured using TFM methods. Maximum traction stress was quantified and the distribution of the data points for each condition can be seen in Figure 3-6 along with representative traction stress maps for pre-scramble transfected and pre-miR-155 transfected samples. There was no significant difference seen in the maximum traction stress exerted by cells in each test group ($P > 0.05$).

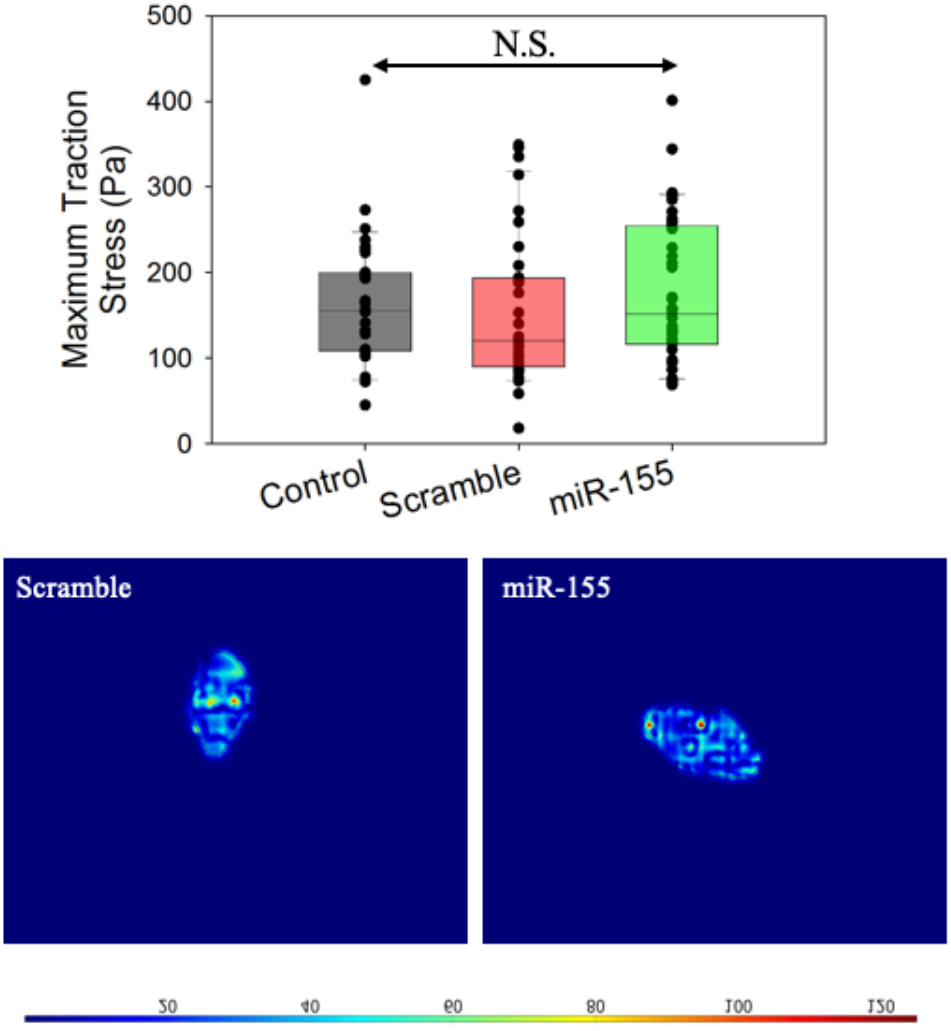

Figure 3-6 TFM Analysis of Increased Mir-155 A549 cells: Maximum traction stress exerted by cells from each treatment condition (top). Representative images of traction stress maps for pre-scramble transfected and pre-miR-155 conditons.

Cytoskeletal imaging of pre-miR-155 transfected cells was done in order to investigate whether miR-155 works to depolymerize the actin-cytoskeleton in lung epithelial cells. Triplicates of both untreated and pre-miR-155 transfected A549 cells were stained for F-actin and DAPI to obtain fluorescent images of their actin-cytoskeleton. Qualitative analysis of the images was used to determine a difference in density and structure of the actin-cytoskeleton. Representative fluorescent images of the actin cytoskeleton for both control and pre-miR-155 transfected is shown in Figure 3-7. Images from the pre-miR-155 transfected group exhibited a slight loss of actin fibers.

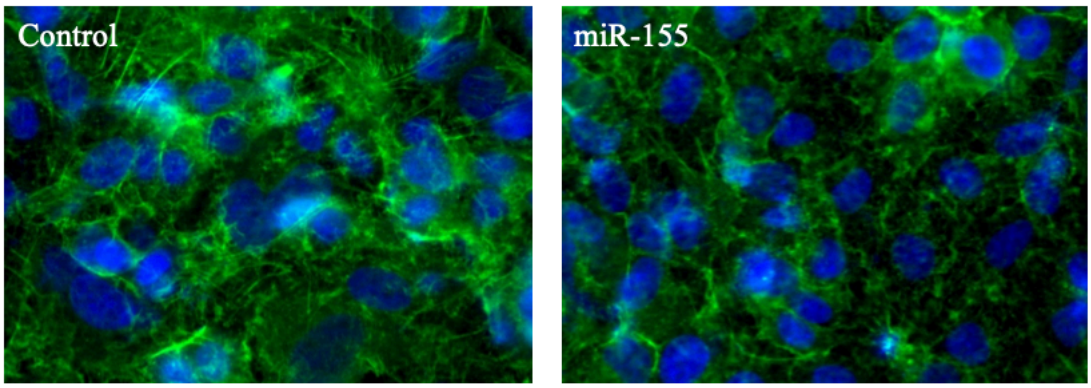

Figure 3-7 Cytoskeletal Imaging of Pre-miR-155 transfected A549 cells: Fluorescent images of actin cytoskeleton for untreated A549 cells (left) and pre-miR-155 transfected A549 cells (right).

In order to identify the specific regulatory targets of miR-155 in lung epithelial cells, several western blots were carried out. The test conditions used were untreated, pre-scramble transfected, and pre-miR-155 transfected A549 cells with triplicate samples of each. Protein contents for the triplicates of each test condition were combined together after the extraction and equalization of the individual samples. Therefore, only three wells were used for samples, one for each test condition. Protein levels were measured for cytoskeletal proteins myosin light chain kinase (MYLK) and ras homolog gene family, member A (RhoA), as well as control protein GAPDH. Exposures for each of the tested proteins are shown in Figure 3-8 on the next page. Visual analysis indicates that MYLK and RhoA may be slightly downregulated by miR-155.

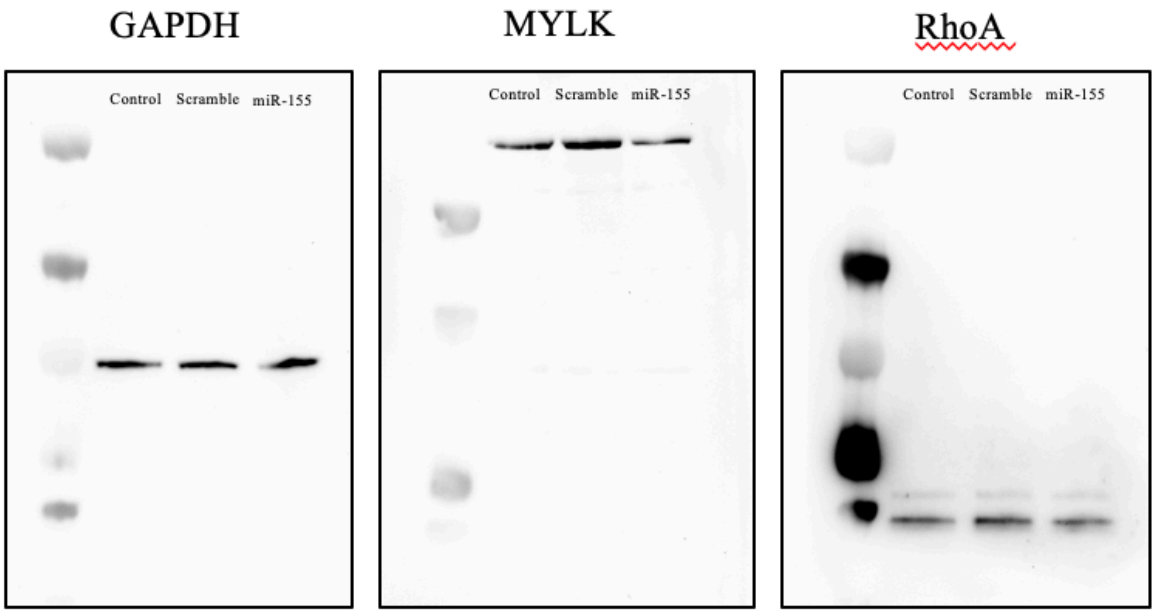

Figure 3-8: Western Blotting to Investigate Regulatory Role of miR-155: Western blots for GAPDH (left), MYLK (middle), and RhoA (right)

It should be noted that western blotting for these samples and proteins (as well as β-actin protein) has been carried out repeatedly, but experimental complications have prevented the generation of any blots that are truly telling of protein levels. More samples will be tested in order to reach a more conclusive basis on this data.

4. Discussion and Conclusions

4.1 Effect of Increased miR-155 on Lung Epithelial Cell Injury and Repair

A bubble flow chamber was used to replicate the injurious forces caused by mechanical ventilation in order to investigate the role of miR-155, and to see if its overexpression can have cytoprotective effects in the lung epithelial cells. Previous studies had shown that miR-155 had been upregulated in response to ventilation [19], leading us to hypothesize that further enhancing miR-155 before injury may help the epithelial cells cope with the forces of ventilation. Transfection techniques proved to be an effective way of significantly increasing miR-155 concentration in A549 lung epithelial cells based on PCR analysis (Figure 3-1). Injury to the lung alveolar epithelial wall is characterized by barrier disruption and increased permeability. This type of injury could be primarily measured in-vitro through quantifying the cell death and detachment for a monolayer of lung epithelial cells. When the transfected cells were cultured to form a monolayer and were exposed to bubble flow, there was a significant decrease in cell death compared to untreated A549 cells exposed to the same bubble flow conditions (Figure 3-2). Whereas increased miR-155 expression did not have a significant impact on the detachment of cells (3-3). This data suggests that miR-155 may have a protective role in the lung epithelial cells and that its overexpression may have therapeutic implications.

The ability of the lung epithelium to heal after enduring the injurious forces of ventilation is another property which miRNAs may be capable of regulating. Wound repair is largely characterized by the migratory and proliferative abilities of cells. Re-growth (re-epithelialization) experiments are able to explore both of these properties to some extent, but do not isolate either. The re-epithelialization experiments showed no significant difference but were largely inconclusive due to inconsistencies in initial injury, as well as due to the variability in the time of

measurements across conditions. These results highlight the need for more systematic ways of efficiently measuring injury (decrease in cell confluence) after exposure to ventilator-like forces. The traction forces which a cell exerts on its substrate give insight into its migratory properties. Experiments carried out for TFM analysis showed no significant difference in the pre-miR-155 transfected cells compared to untreated control cells. This study used a high sample size of cells therefore the confidence of these results is relatively high, but repeated TFM experiments may be desirable due to the fact that only one sample of each condition was used. Results from the MTT proliferation assay showed no significant difference in proliferative abilities of the lung epithelial cells based on miR-155 expression levels. To fully rule out would healing as a regulatory pathway for miR-155, migration assays as well as repeated regrowth and TFM experiments should be carried out in the future.

4.2 Effect of Increased miR-155 on Lung Epithelial Cell Morphology

Previous work has demonstrated the importance of the epithelial cell morphology in resisting the injurious forces of mechanical ventilation [10-15]. Specifically, it was seen that a more compliant epithelial cell decreases the shear stress that the cell is subject to during ventilation [11]. Therefore, we hypothesized that the decreased injury seen in epithelial cells with increased expression of miR-155 may be due to changes in morphology. AFM experiments showed that pre-miR-155 transfected A549 cells had a significantly lower young's modulus and taller cell height than untreated control A549 cells. These findings are consistent with previous studies which claimed that a softer cell is less susceptible to shear forces [10]. Interestingly, the pre-miR-155 transfected cells were measured to be taller, which is a contradiction to previous work which showed taller cells tended to be more susceptible to injury (14). Overall, these findings suggest that miR-155 targets morphology regulating pathways.

4.3 Mechanism of miR-155 in Lung Epithelial Cell

Softening of the cell morphology is generally due to regulation of the cytoskeleton. Also, previous work has suggested that a less fiber-like network may promote cell survival during ventilation and has shown that a depolymerized actin cytoskeleton increases viability and adhesion when subject to ventilation forces [13,15]. This along with the AFM data collected led to investigation of the cytoskeleton. Actin cytoskeleton images of pre-miR-155 transfected cells showed slightly less actin density when compared to control. These results suggest that miR-155 deregulates cytoskeletal actin, but visual analysis is not significant enough to draw conclusions especially when the differences are small. Western blot data looking at cytoskeletal proteins had similar results in that they suggested that based on qualitative analysis there may be slightly less levels of RhoA and MYLK in pre-miR-155 transfected cells. Regardless of what the results suggest, these experiments should be repeated and quantified to confirm statistical significance. Until this significance is confirmed, we cannot conclude that miR-155 deregulation of the actin cytoskeleton is the reason that miR-155 mitigates ventilator induced injury to lung epithelial cells. Future experiments should aim to characterize the effect of miR-155 on the tight junctions in A549 epithelial cells and should also attempt to identify the proteins which miR-155 targets.

References:

[1] Ware, L. B., & Matthay, M. A. (May 04, 2000). Medical Progress: The Acute Respiratory Distress Syndrome. *The New England Journal of Medicine, 342,* 1334-1349.

[2] Slutsky, A. S., & Ranieri, V. M. (January 01, 2013). Ventilator-induced lung injury. *The New England Journal of Medicine, 369,* 22, 2126-36.

[3] Pinhu, L., Whitehead, T., Evans, T., & Griffiths, M., (January 01, 2003). Ventilator-associated lung injury. *Lancet, 361*, 9354, 332–340.

[4] Levy, M. M. (January 01, 2004). PEEP in ARDS--how much is enough? *The New England Journal of Medicine, 351,* 4, 389-91.

[5] Ghadiali, S. N., & Gaver, D. P. (November 30, 2008). Biomechanics of liquid-epithelium interactions in pulmonary airways. *Respiratory Physiology & Neurobiology, 163,* 1-3.

[6] Bilek, A. M., Dee, K. C., & Gaver, D. P. (January 01, 2003). Mechanisms of surface-tension-induced epithelial cell damage in a model of pulmonary airway reopening. *Journal of Applied Physiology, 94,* 2, 770-83.

[7] D'Angelo, E., Pecchiari, M., Saetta, M., Balestro, E., & Milic-Emili, J., (January 01, 2004). Dependence of lung injury on inflation rate during low-volume ventilation in normal open- chest rabbits *Journal of Applied Physiology, 97,* 1, 260-8.

[8] D'Angelo, E., Pecchiari, M., & Gentile, G. (January 01, 2007). Dependence of lung injury on surface tension during low-volume ventilation in normal open-chest rabbits. *Journal of Applied Physiology, 102,* 1, 174-82.

[9] Lewis, J. F., & Veldhuizen, R. (January 01, 2003). The role of exogenous surfactant in the treatment of acute lung injury. *Annual Review of Physiology, 65,* 613-642.

[10] Jacob, A. M., & Gaver, D. P. (January 01, 2005). An investigation of the influence of cell topography on epithelial mechanical stresses during pulmonary airway reopening. *Physics of Fluids, 17,* 3.

[11] Dailey, H. L., Yalcin, H. C., & Ghadiali, S. N. (June 01, 2007). Fluid-structure modeling of flow-induced alveolar epithelial cell deformation. *Computers and Structures, 85,* 1066-1071.

[12] Dailey, H. L., & Ghadiali, S. N. (June 01, 2010). Influence of power-law rheology on cell injury during microbubble flows. *Biomechanics and Modeling in Mechanobiology, 9,* 3, 263-279.

[13] Yalcin, H. C., Perry, S. F., & Ghadiali, S. N. (January 01, 2007). Influence of airway diameter and cell confluence on epithelial cell injury in an in vitro model of airway reopening. *Journal of Applied Physiology, 103,* 5, 1796.

[14] Dailey, H. L., Ricles, L. M., Yalcin, H. C., & Ghadiali, S. N. (January 01, 2009). Image-based finite element modeling of alveolar epithelial cell injury during airway reopening. *Journal of Applied Physiology, 106,* 1, 221-32.

[15] Yalcin, H. C., HaIIow, K. M., Wang, J., Wei, M. T., Ou-Yang, H. D., & Ghadiali, S. N. (November 01, 2009). Influence of cytoskeletal structure and mechanics on epithelial cell injury during cyclic airway reopening. *American Journal of Physiology: Lung Cellular & Molecular Physiology, 41,* 5.

[16] Ressler, B., & Lee, R. T. (June 01, 2000). Molecular responses of rat tracheal epithelial cells to transmembrane pressure. *American Journal of Physiology, 278,* 6.

[17] Ridge, K. M., Linz, L., Flitney, F. W., Kuczmarski, E. R., Chou, Y. H., Omary, M. B., Sznajder, J. I., ... Goldman, R. D. (January 01, 2005). Keratin 8 phosphorylation by protein kinase C delta regulates shear stress-mediated disassembly of keratin intermediate filaments in alveolar epithelial cells. *The Journal of Biological Chemistry, 280,* 34, 30400-5.

[18] D'Angelo, E., Koutsoukou, A., Della, V. P., Gentile, G., & Pecchiari, M. (January 01, 2008). Cytokine release, small airway injury, and parenchymal damage during mechanical ventilation in normal open-chest rats. *Journal of Applied Physiology, 104,* 1, 41-9.

[19] Huang, Y., Haas, C., & Ghadiali, S. N. (December 01, 2010). Influence of Transmural Pressure and Cytoskeletal Structure on NF-κB Activation in Respiratory Epithelial Cells. *Cellular and Molecular Bioengineering, 3,* 4, 415-427.

[20] Sevignani, C., Calin, G. A., Siracusa, L. D., & Croce, C. M. (March 01, 2006). Mammalian microRNAs: a small world for fine-tuning gene expression. *Mammalian Genome : Incorporating Mouse Genome, 17,* 3, 189-202.

[21] Ferruelo, A., Peñuelas, O., & Lorente, J. A. (January 01, 2018). MicroRNAs as biomarkers of acute lung injury. *Annals of Translational Medicine, 6,* 2.

[22] Vaporidi, K., Vergadi, E., Kaniaris, E., Hatziapostolou, M., Lagoudaki, E., Georgopoulos, D., Zapol, W. M., ... Iliopoulos, D. (January 01, 2012). Pulmonary microRNA profiling in a mouse model of ventilator-induced lung injury. *American Journal of Physiology, 303,* 2.

[23] Han, Z., Chen, Y., Zhang, Y., Wei, A., Zhou, J., Li, Q., & Guo, L. (October 01, 2017). MiR-21/PTEN Axis Promotes Skin Wound Healing by Dendritic Cells Enhancement. *Journal of Cellular Biochemistry, 118,* 10, 3511-3519.

[24] Huang, Y., Crawford, M., Higuita-Castro, N., Nana-Sinkam, P., & Ghadiali, S. N. (January 01, 2012). miR-146a regulates mechanotransduction and pressure-induced inflammation in small airway epithelium. *Faseb Journal: Official Publication of the Federation of American Societies for Experimental Biology, 26,* 8, 3351-64.

[25] Weber, M., Kim, S., Patterson, N., Rooney, K., & Searles, C. D. (January 01, 2014). MiRNA-155 targets myosin light chain kinase and modulates actin cytoskeleton organization in endothelial cells. *American Journal of Physiology, 306,* 4.

[26] Higuita-Castro, N., Shukla, V. C., Mihai, C., & Ghadiali, S. N. (December 01, 2016). Simvastatin Treatment Modulates Mechanically-Induced Injury and Inflammation in Respiratory Epithelial Cells. *Annals of Biomedical Engineering: The Journal of the Biomedical Engineering Society, 44,* 12, 3632-3644.

[27] Hammer, A. M., Sizemore, G. M., Shukla, V. C., Avendano, A., Sizemore, S. T., Chang, J. J., Kladney, R. D., ... Ostrowski, M. C. (January 01, 2017). Stromal PDGFR-α Activation Enhances Matrix Stiffness, Impedes Mammary Ductal Development, and Accelerates Tumor Growth. *Neoplasia, 19,* 6, 496-508.